JPEDAV (2009) 30:146–156
DOI: 10.1007/s11669-009-9467-4
1547-7037 ©ASM International

Thermodynamics and Constitution of Mg-Al-Ca-Sr-Mn Alloys: Part I. Experimental Investigation and Thermodynamic Modeling of Subsystems Mg-Ca-Sr and Al-Ca-Sr

A. Janz and R. Schmid-Fetzer

(Submitted June 25, 2008; in revised form October 2, 2008)

Ternary Mg-Ca-Sr and Al-Ca-Sr phase transitions were experimentally investigated by differential thermal analysis; phase formation in slowly solidified samples was analyzed with scanning electron microscopy and electron probe microanalysis. Significant mutual ternary solid solubilities of pertinent intermetallic phases are revealed and quantitatively introduced in thermodynamic descriptions that were developed for the Mg-Ca-Sr and the Al-Ca-Sr systems. Calcium and strontium are two chemically rather similar alloying elements. Even so, nontrivial ternary phase equilibria occur in these systems, and these alloys should not be simplified as "binary" Mg-(Ca + Sr) or Al-(Ca + Sr) alloys. Experimental work was limited, and, thus, reported results are affected by a relatively high level of uncertainty.

Keywords CALPHAD approach, experimental phase equilibria, invariant equilibria, liquidus surface, phase diagram microstructure

1. Introduction

The global goal of this study is to generate a thermodynamic description of phase equilibria in the Mg-Al-Ca-Sr-Mn alloy system, validated with an emphasis to Mg-rich alloys. These alloys are important for an extension of the portfolio of lightweight magnesium alloys, where the alloying elements are usually denoted by the ASTM letter code for Al (A), Ca (X), Sr (J), Mn (M). This covers the area of advanced creep-resistant alloys of the AJ and AJX series, but also to the modification of AM using Ca and Sr for improved properties. Combined with a major database including the important component Zn (Z),[1] it will also cover such modifications involving the popular Mg alloy series AZ. Thus, thermochemical calculations will be enabled in the (Mg)-AZMXJ alloy systems, which are an important tool for focused alloy development and process optimization.[2]

The main focus is presently on the Mg-Al-Ca-Sr phase equilibria, where the investigation of two of the ternary subsystems were recently finished, namely Mg-Al-Ca[3] and Mg-Al-Sr.[4] The remaining ternary systems Mg-Ca-Sr and Al-Ca-Sr involve two chemically rather similar alloying elements, Ca and Sr. Even so, it will be shown that nontrivial ternary phase equilibria occur in these systems. This highlights the need to study the ternary interactions in detail rather than summing up the Ca and Sr contents and treating these alloys as simplified "binary" Mg-(Ca + Sr) and Al-(Ca + Sr) alloys. The purpose of part I of this work is to generate a consistent thermodynamic description of the phase equilibria in both ternary systems by combining experimental work with thermodynamic modeling.

A. Janz and **R. Schmid-Fetzer,** Institute of Metallurgy, Clausthal University of Technology, Robert-Koch-Str. 42, D-38678 Clausthal-Zellerfeld, Germany. Contact e-mail: schmid-fetzer@tu-clausthal.de.

2. Experimental Data and Thermodynamic Descriptions in the Literature

Experimental information on ternary phase equilibria or thermodynamics for these two systems is scarce. No data could be found in the literature for the ternary Mg-Ca-Sr system, and only one study relates to the Al-Ca-Sr system. Zhang et al.[5] investigated six alloys in the section $Sr_{1-x}Ca_xAl_2$ ($0 \le x \le 1$) with x-ray diffraction (XRD). Their main interest was in the hydrogenation behavior of these alloys, but they also characterized the alloys before exposure to hydrogen. Based on the variation of lattice parameters of the terminal compounds, which crystallize in significantly different structures, they determined a small solubility of Ca in the orthorhombic Zintl phase Al_2Sr (space group *Imma*, Pearson symbol *oI*12) and a very large Sr solubility in the cubic Laves phase *C*15-Al_2Ca (space group $Fd\bar{3}m$, Pearson symbol *cF*24). A narrow two-phase region was found to exist between these phases. The six samples were analyzed in as-cast condition after four times remelting in an arc furnace.

Ternary thermodynamic calculations reported in the literature are all based on extrapolations of Calphad-type assessments of the binary edge systems. For the Mg-Ca-Sr

system Zhong et al.[6] performed such calculations, using the assumption of ideal mixing between the *C*14 Laves phases Mg_2Ca and Mg_2Sr and employing a reassessed binary Ca-Sr dataset. Aljarrah and Medraj[7] reassessed the three binaries using the modified quasi-chemical model. With these datasets and Kohler-based extrapolation for the ternary liquid phase they calculated some Mg-Ca-Sr liquidus projections assuming three different scenarios: (a) zero solubility between Mg_2Ca and Mg_2Sr, (b) a random solution model for the liquid phase, and (c) complete solid solubility between Mg_2Ca and Mg_2Sr.

These authors[8] applied the same procedures also to the Al-Ca-Sr system. They converted existing thermodynamic descriptions to the modified quasi-chemical model in a reoptimization of the binary subsystems. No ternary solubilities of the binary phases were considered in that work; specifically, the only experimental work in that system, revealing extended solutions on the Al_2Ca-Al_2Sr section,[5] was not considered.

3. Experimental Study

3.1 Sample Preparation

In the present study we have used such ternary thermodynamic calculations based on extrapolations of binary datasets to identify key samples. Two ternary alloy compositions were selected in each system to investigate the ternary phase transitions with differential thermal analysis (DTA) and also the ternary solubilities of the binary phases in these slowly cooled alloys. One additional sample in the Al-Ca-Sr system (sample ACS2, Al60Ca12.5Sr27.5, wt.%) was preheated at 1000 °C for 30 min, then cooled down to 500 °C, held at that temperature for 20 days and quenched. The procedure of identifying key samples for probing important invariant reactions is elaborated in part II of this study.[9]

All samples were prepared from Mg granules (99.98 wt.%, Alfa, Karlsruhe, Germany), Al pieces (99.999/99.997 wt.%, Alfa, Karlsruhe, Germany), Ca pieces (99.99 wt.%, Aldrich-APL, Urbana, IL), and Sr pieces (99.99 wt.%, Aldrich-APL, Urbana, IL). All purity designations are related to the metal basis. The weighed sample materials were pressed carefully to pellets that were then sealed in Ta capsules by careful electric arc welding under argon at 1 bar; the procedure is described in more detail elsewhere.[10]

After testing the tightness of the capsules in a separate furnace, differential thermal analysis was carried out using a Netzsch DTA 404 apparatus (Netzsch GmbH, Selb, Germany). The measurements were repeated in three cycles for each of the two heating/cooling rates of 5 and 1 K/min. A typical sample weight was about 250 mg. The overall uncertainty of DTA measurements for temperature determination was estimated to be ±2 K for strong and clear signals and ±5 K for weak and diffuse signals.

The DTA sample compositions are given in Table 1. Microstructural analysis was done for all samples after 1 K/min cooling with scanning electron microscopy in backscattered electron contrast (SEM/BSE); local chemical compositions were identified with electron probe microanalysis (EPMA/EDX and WDX), also for sample ACS2.

3.2 Experimental Results

3.2.1 Mg-Ca-Sr Samples. The DTA results are given in Table 1. Figure 1 shows the microstructure of sample MCS1. Large platelike particles of $Mg_{17}Sr_2$ and smaller

Table 1 Temperatures extracted from the DTA signals obtained by thermal analysis in the Mg-Ca-Sr and the Al-Ca-Sr system and their interpretation

No.	Sample composition, wt.%	Thermal signal, °C			Interpretation
		Heating	Cooling	Evaluated	Calculated equilibrium temperature, °C; phase boundary or invariant reaction
MCS1	Mg70.9	552 w	553 w	553	566 L/L + *C*14
	Ca13.9	533 w	530 w	533	535 L + *C*14/L + *C*14 + $Mg_{17}Sr_2$
	Sr15.2	512 s	511 s	512	510 E1
MCS2	Mg57.8	603 s	595 w	603	?
	Ca03.5	587 w	587 s	587	585 L/L + *C*14
	Sr38.7	…	…	…	583 L + *C*14/L + *C*14 + $Mg_{38}Sr_9$
		566 w	566 w	566	564 U2
ACS1	Al79.3	…	890 s	890	868 L/L + Al_4Sr
	Ca6.5	620 s	618 s(a)	619	620 L + Al_4Sr/L + Al_4Sr + (Al)
	Sr14.2	…	(618 s)(a)	…	614 U2
ACS3	Al49.7	965 w	965 w	965	974 L/L + *C*15
	Ca15.7	955 s	950 s	953	939.0 L + *C*15/L + *C*15 + Al_4Sr
	Sr34.6	…	…	…	938.6 L + *C*15 + Al_4Sr/*C*15 + Al_4Sr

w, weak and diffuse signal; s, strong and clear signal; (a), double peak; …, not detected. Invariant reactions were recognized from the peak shape

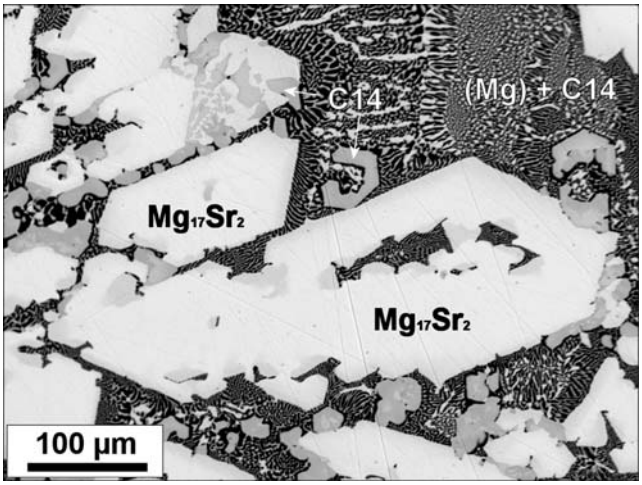

Fig. 1 Scanning electron micrograph (SEM/BSE) of sample MCS1 after slow cooling in DTA with 1 K/min

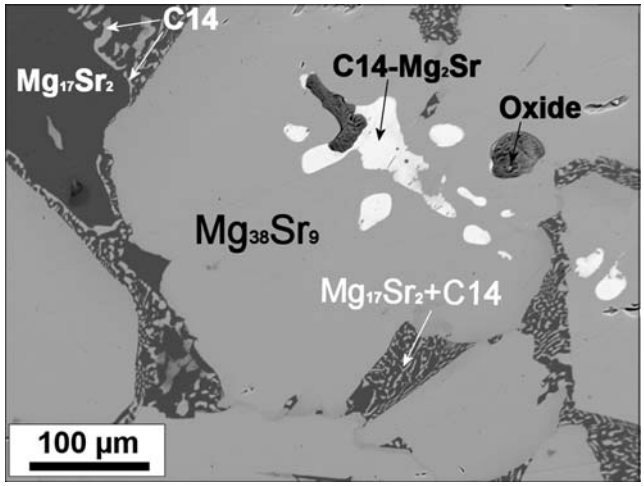

Fig. 2 Scanning electron micrograph (SEM/BSE) of sample MCS2 after slow cooling in DTA with 1 K/min

ones of *C*14-Mg_2(Ca,Sr) can be seen. Also, a significant amount of (Mg) + *C*14 (+$Mg_{17}Sr_2$) eutectic microstructure was formed in the final step of solidification. Microprobe analysis identified less than 10 wt.% of Sr in *C*14 and less than 5 wt.% of Ca in $Mg_{17}Sr_2$, an even smaller solubility of Ca in the (Mg) phase and no Sr solubility in (Mg); the analysis was done in a different part of the sample with larger (Mg) grains. The entirety of microprobe data is shown later in the isothermal phase diagram sections at 500 °C.

Sample MCS2 was located close to the Mg-Sr binary edge in order to check the second important invariant reaction, identified later as U2. The microstructure in Fig. 2 shows large grains of $Mg_{38}Sr_9$ with occasional inclusion of smaller Sr-rich *C*14-Mg_2(Ca,Sr) particles, appearing bright. Additional $Mg_{17}Sr_2$ areas and a fine $Mg_{17}Sr_2$ + *C*14 microstructure are present. It is noteworthy that the *C*14 in the fine microstructure has a significantly higher Ca content compared with that of the *C*14 found inside the $Mg_{38}Sr_9$ particles. The microprobe data support a complete solid solubility of *C*14-Mg_2(Ca,Sr). This is discussed later in detail.

3.2.2 Al-Ca-Sr Samples. The DTA results of two alloys are given in Table 1. Table 2 summarizes the phases detected by SEM/BSE and EPMA in all three samples in the Al-Ca-Sr system, including the "equilibrated" ACS2 sample.

Sample ACS1 is located within the expected equilibrium of (Al) + Al_4Sr + Al_4Ca. These three phases actually form in majority as can be seen in the micrograph in Fig. 3. A contamination with Al-Ta phases due to the reaction with the Ta capsule is observed. The sample was exposed to a maximum temperature of 930 °C for 30 min during the six DTA cycles. The attack of this Al-rich sample on the capsule is strong since the chemical activity, a_{Al}, is high with virtually pure (Al) present. EPMA showed that both intermetallic phases, Al_4Sr and Al_4Ca, exhibit significant ternary solubilities in the Ca-Sr direction. The white particles are identified as Al_3Ta. They are often surrounded by an unknown ternary phase with approximate composition

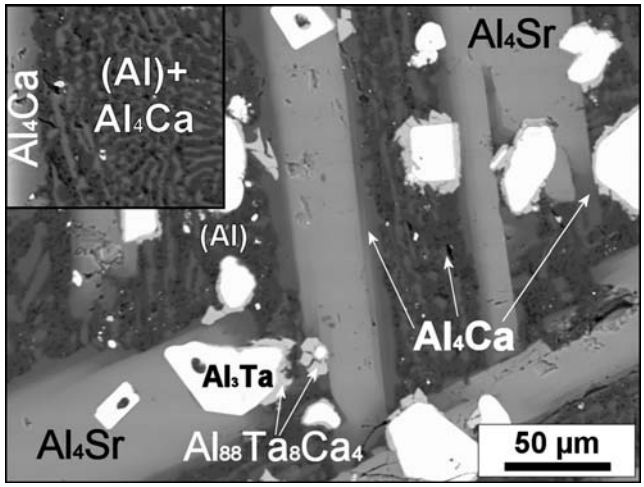

Fig. 3 Scanning electron micrograph (SEM/BSE) of sample ACS1 after slow cooling in DTA. Inset shows a different part of that sample at same magnification

Table 2 Phases detected in Al-Ca-Sr samples using SEM/BSE and EPMA

Sample	Phases
ACS1	Al_4Sr + Al_4Ca + (Al) {+Al_3Ta + $Al_{88}Ta_8Ca_4$}
ACS2	(Al) + Al_4Sr + *C*15 + Al_7Sr_8 {+CaO?}
ACS3	Al_4Sr + *C*15

of $Al_{88}Ta_8Ca_4$. Al_4Sr formed as primary phase and in the shape of solid bars as already known from the investigations of the Mg-Al-Sr phase equilibria.[4] The Al_4Ca phase formed a layer on the Al_4Sr bars and finally a eutectic microstructure with the fcc-(Al), which is more clearly seen in the inset of Fig. 3, showing a different part of that sample at same magnification.

Figure 4 shows the microstructure of sample ACS3 after final cooling from 980 °C with 1 K/min in DTA. Obviously the mass contrast between the phases present is very small, in most cases not discernible. Using light optical microscopy (LOM) nuances in contrast were observed as shown in the inset of Fig. 4. With EPMA it was possible to identify two phases with ternary solubility: Al_4Sr (with Ca dissolved) and the *C*15 Laves phase Al_2(Ca,Sr).

The microstructure of sample ACS2 after heating at 500 °C for 20 days in a Ta capsule is presented in Fig. 5. The sample has not reached equilibrium since four phases can be identified: (Al), Al_4Sr, *C*15, and Al_7Sr_8. This order represents the increasing Sr content in these phases. Even though equilibrium is not attained, the ternary solubilities of the binary phases measured in this sample with EPMA are useful to support the solid solubility ranges or estimate its value in Al_7Sr_8. It was not possible to analyze the somewhat grainy structure in the lower middle part of the image. In contrast to sample ACS1, the capsule has not been affected and Al-Ta phases were not found, possibly because of the lower Al content of 60 compared to 79.3 wt.% Al.

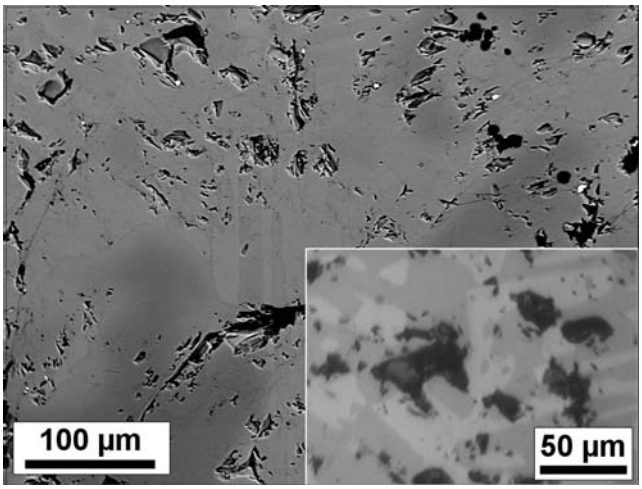

Fig. 4 Scanning electron micrograph (SEM/BSE) of sample ACS3 after slow cooling in DTA. The inset shows the microstructure with LOM

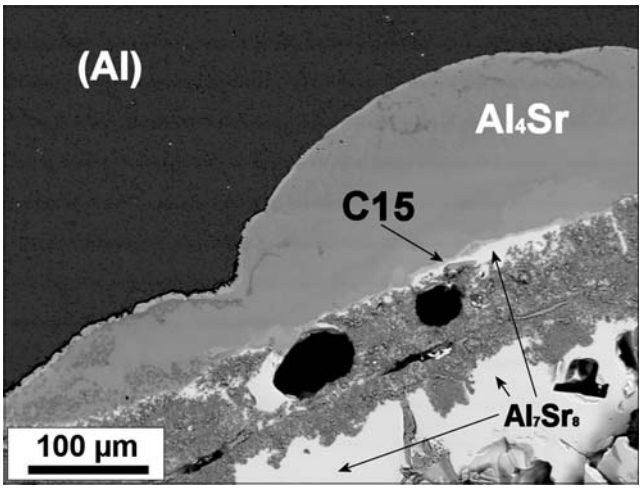

Fig. 5 Scanning electron micrograph (SEM/BSE) of sample ACS2 after heating at 500 °C for 20 days

4. Thermodynamic Modeling

Table 3 summarizes the sources of thermodynamic descriptions of the binary subsystems accepted in the present study. In the Mg-Ca system we slightly adjusted the parameters to incorporate the improved C_p function of *C*14-Mg_2Ca.[11] The ternary interactions were extrapolated from these descriptions in the preliminary calculations used to identify key samples. The software package Pandat[12,13] was used for all calculations in this work.

The Gibbs energy function $G_i^{0,\phi}(T) = G_i^{\phi}(T) - H_i^{SER}$ for the element *i* (*i* = Al, Ca, Mg, Sr) in the ϕ phase [ϕ = face-centered cubic (fcc) (Al, αCa, αSr), body-centered cubic (bcc) (βCa, βSr) and closed packed hexagonal (cph) (Mg), or liquid] is described by:

$$G_i^{0,\phi}(T) = a + b \cdot T + c \cdot T \cdot \ln T + d \cdot T^2 + e \cdot T^3 + f \cdot T^{-1} + g \cdot T^7 + h \cdot T^{-9} \quad \text{(Eq 1)}$$

where H_i^{SER} is the molar enthalpy of the stable element reference (SER) at 298.15 K and 1 bar, and *T* is the absolute temperature. These unary Gibbs energy functions for Al, Ca, Mg, and Sr are taken from the SGTE compilation by Dinsdale.[14]

The liquid, fcc (Al, αCa, αSr), bcc (βCa, βSr), and cph (Mg) solution phases are described by the substitutional solution model. For the liquid phase (Liq) in the Mg-Ca-Sr system, the molar Gibbs energy is expressed by following Redlich-Kister-type equation:

$$G^{Liq} = x_{Ca}G_{Ca}^{0,Liq} + x_{Mg}G_{Mg}^{0,Liq} + x_{Sr}G_{Sr}^{0,Liq} + {}^{E}G^{bin,Liq} + RT\left(x_{Ca}\ln x_{Ca} + x_{Mg}\ln x_{Mg} + x_{Sr}\ln x_{Sr}\right) \quad \text{(Eq 2)}$$

in which ${}^{E}G^{bin,Liq}$ describes the excess contribution from all binary interactions, *R* is the gas constant, and x_{Ca}, x_{Mg}, and x_{Sr} are the molar fractions of Ca, Mg, and Sr. An analogous equation is used for the solution phases in the Al-Ca-Sr system. No ternary interaction parameter was found to be necessary for any of the solution phases (liquid, fcc, bcc, cph).

Based on the experimental results from DTA, SEM/BSE, and EPMA presented previously, limited ternary solubilities were introduced in the description of most binary

Table 3 Sources of binary thermodynamic descriptions for the ternary Mg-Ca-Sr and Al-Ca-Sr systems

	Mg	Al	Ca
-Ca	Agarwal et al.[17]	Kevorkov et al.[19]	…
-Sr	Zhong et al.[6]	Zhong et al.[20]	Zhong et al.[21]

intermetallic phases. These are the Mg-Sr based phases $Mg_{17}Sr_2$ and $Mg_{38}Sr_9$, the Al-Ca phases Al_4Ca and *C*15-Al_2Ca, and the Al-Sr phases Al_4Sr, Al_2Sr and Al_7Sr_8. All these phases were modeled as line compounds $(Mg)_m(Ca,Sr)_n$ or $(Al)_m(Ca,Sr)_n$ to reflect the experimentally observed ternary solubilities.

As an example, the Gibbs energy (per mole of atoms) for $Mg_{17}Sr_2$ using the model $(Mg)_{17}(Ca,Sr)_2$ in the compound energy formalism[15] is expressed by

$$G^{Mg_{17}Sr_2} = y_{Ca}G^{0,Mg_{17}Sr_2}_{Mg:Ca} + y_{Sr}G^{0,Mg_{17}Sr_2}_{Mg:Sr} + \frac{2}{19}RT(y_{Ca}\cdot\ln y_{Ca} + y_{Sr}\cdot\ln y_{Sr}) + y_{Ca}\cdot y_{Sr}\cdot L^{Mg_{17}Sr_2}_{Mg:Ca,Sr} \quad \text{(Eq 3)}$$

in which y_{Ca} and y_{Sr} are the site fractions of Ca and Sr on the sublattice with variable composition. The parameters $G^{0,\phi}_{i:j}$ (also called compound energies) are expressed relative to the Gibbs energies of the pure elements (Ca-fcc, Mg-cph, Sr-fcc) at the given temperature *T*. The proper compound energy $G^{0,Mg_{17}Sr_2}_{Mg:Sr}$ represents the stable binary phase $Mg_{17}Sr_2$. The value is taken from the binary description of the Mg-Sr system.[6] The parameter $G^{0,Mg_{17}Sr_2}_{Mg:Ca}$ represents the counter phase of the solution range that is metastable in the Mg-Ca system and is to be optimized. The parameters describing ternary interactions essentially within the sublattice, such as $L^{Mg_{17}Sr_2}_{Mg:Ca,Sr}$, could be set to zero for all these phases with limited ternary solubility.

The two stable Laves phases *C*14-Mg_2Ca and *C*14-Mg_2Sr exhibit a complete mutual solubility. They crystallize in the same hexagonal structure (Pearson symbol *hP*12, prototype $MgZn_2$) and are modeled as one phase with the model $(Mg)_2(Ca,Sr)$. Again, it was not necessary to introduce an interaction parameter $\left(L^{C14}_{Mg:Ca,Sr} = 0\right)$, and thus an ideal solution is used.

Both Al_4Ca and Al_4Sr have the same body-centered tetragonal crystal structure (Pearson symbol *tI*10, prototype $BaAl_4$). Therefore these two phases might have been merged into one phase $Al_4(Ca,Sr)$. The results from SEM/BSE and EPMA of sample ACS1, however, show that no *complete* solubility exists between the two binary end members. A merged model for this phase would have to reproduce this asymmetric solid-state demixing, which is fairly complex to be realized. For the sake of simplicity it was decided to keep both phases in separate models.

On the Al_2Ca-Al_2Sr section, it is not possible to merge the Laves phase *C*15-Al_2Ca (Pearson symbol *cF*24, prototype $MgCu_2$) and the Zintl phase Al_2Sr (Pearson symbol *oI*12, prototype $CeCu_2$) because of the different crystal structures. The values of all parameters optimized for the Al-Ca-Sr and Mg-Ca-Sr systems are given in Table 4. Parameters that have already been published in other journal articles are not listed. The thermodynamic modeling is given in more detail in a thesis work.[16]

The results of the final thermodynamic modeling are presented in the calculated phase diagrams shown below in the discussion of both ternary systems. The calculated invariant reactions involving the liquid phase are listed in Table 5 for the Mg-Ca-Sr system and in Table 6 for the Al-Ca-Sr system. The results are compared with the experimental temperatures. Table 7 shows the calculated

Table 5 Invariant four-phase reactions involving the liquid phase in the ternary Mg-Ca-Sr system

Type	Reaction(a)	*T*/°C calculated	*T*/°C experimental
U1	L + $Mg_{23}Sr_6$ ↔ *C*14 + $Mg_{38}Sr_9$	594	…
U2	L + $Mg_{38}Sr_9$ ↔ $Mg_{17}Sr_2$ + *C*14	564	566
E1	L ↔ (Mg) + $Mg_{17}Sr_2$ + *C*14	510	512
U3	L + β(Ca,Sr) ↔ a(Ca,Sr) + *C*14	443	…

(a) Generic notation bcc = β(Ca,Sr) and fcc = α(Ca,Sr) is used in diagrams

Table 6 Invariant four-phase reactions involving the liquid phase in the ternary Al-Ca-Sr system

Type	Reaction	*T*/°C calculated	*T*/°C experimental
U1	L + Al_4Sr ↔ *C*15 + Al_2Sr	907	…
P1	L + Al_4Sr + *C*15 ↔ Al_4Ca	712	…
U2	L + Al_4Sr ↔ Al_4Ca + (Al)	614	(618)
U3	L + Al_2Sr ↔ *C*15 + Al_7Sr_8	604	…
U4	Al_3Sr_8 + β(Ca,Sr) ↔ a(Ca,Sr) + L	554	…
U5	L + β(Ca,Sr) ↔ a(Ca,Sr) + Al_3Ca_8	451	…
U6	L + Al_3Sr_8 ↔ Al_7Sr_8 + α(Ca,Sr)	405	…
U7	L + *C*15 ↔ Al_7Sr_8 + AlCa	360	…
U8	L + AlCa ↔ Al_7Sr_8 + Al_3Ca_8	322	…
E1	L ↔ Al_7Sr_8 + Al_3Ca_8 + α(Ca,Sr)	235	…

Table 4 Ternary thermodynamic parameters for the Al-Ca-Sr and Mg-Ca-Sr systems

Phase name	Model	Parameters, J/mol
*C*15	$(Al)_{0.666667}(Ca,Sr)_{0.333333}$	${}_{15,0:CSrAl}G = -27{,}900 + 2{*}T + 0.666667{*} + 0.333333{*}\ {}_{fccAl}G_{,0fccSr}G_{,0}$
Al_4Ca	$(Al)_{0.8}(Ca,Sr)_{0.2}$	${}_{CaAlSrAl}G_{4,0:} = -26{,}800 + 10{*}T + 0.8{*} + 0.2{*}\ {}_{fccAl}G_{,0fccSr}G_{,0}$
Al_2Sr	$(Al,Mg)_2(Ca,Sr)$	${}_{SrAlCaAl}G_{2,0:} = -83{,}468 + 18.32{*}T + 2{*} + {}_{fccAl}G_{,0fccCa}G_{,0}$
Al_4Sr	$(Al,Mg)_4(Ca,Sr)$	${}_{SrAlCaAl}G_{4,0:} = -103{,}000 + 32{*}T + 4{*} + {}_{fccAl}G_{,0fccCa}G_{,0}$
Al_7Sr_8	$(Al)_7(Ca,Sr)_8$	${}_{87,0:SrAlCaAl}G = -285{,}000 + 7{*} + 8{*}\ {}_{fccAl}G_{,0fccCa}G_{,0}$
$Mg_{17}Sr_2$	$(Al,Mg)_{17}(Ca,Sr)_2$	${}_{217,0:SrMgCaMg}G = -73{,}000 + 40{*}T + 17{*} + 2{*}\ {}_{cphMg}G_{,0fccCa}G_{,0}$
$Mg_{38}Sr_9$	$(Al,Mg)_{38}(Ca,Sr)_9$	${}_{938,0:SrMgCaMg}G = -205{,}000 + 120{*}T + 38{*} + 9{*}\ {}_{cphMg}G_{,0fccCa}G_{,0}$

compositions of the phases involved at the important and also well-established reaction E1 in the Mg-Ca-Sr system. There is only one maximum in the monovariant lines in the Al-Ca-Sr system, which is calculated to occur at 939 °C for the reaction L ↔ Al_4Sr + *C*15. There is no maximum at all involving the liquid phase in the Mg-Ca-Sr system, in contrast to the related Mg-Al-Ca and Mg-Al-Sr systems.

5. Discussion

5.1 The Mg-Ca-Sr Phase Equilibria

The predominant primary crystallizing phase in the Mg-Ca-Sr system is the *C*14-Mg_2(Ca,Sr) as demonstrated in the calculated projection of the liquidus surface in Fig. 6. Due to the complete mutual solubility of Ca and Sr in this phase the primary *C*14 field extends from the binary Mg-Ca to the Mg-Sr edge. The only invariant reaction involving the (Mg) phase is the ternary eutectic E1 at 510 °C. At higher Sr content two U-type transformations occur. The reactions E1 and U2 are the most relevant for a quantitative control of the Mg-rich equilibria. Their calculated invariant temperatures agree within 2 K with the experimental data as shown in Table 5. The primary precipitation observed in the microstructures of the two samples in Fig. 1 and 2 is also consistent with the calculation. Even though $Mg_{17}Sr_2$ forms the more dominant blocky particles, the *C*14 particles may also be found inside $Mg_{17}Sr_2$, but not the other way around. Thermodynamic calculation for alloy MCS1 also supports the larger fraction of $Mg_{17}Sr_2$ phase, forming essentially during the monovariant reaction L → $Mg_{17}Sr_2$ + *C*14.

The calculated phase sequence during solidification is given in the right column of Table 1.

One additional transition reaction, U3, appears close to the Ca corner. This reaction is almost degenerated and originates from the bcc-fcc transformation of Ca and Sr, even though small amounts of liquid and *C*14 take part in this reaction as well. The Mg-poor part of the phase diagram is at least qualitatively correct since it is based on an extrapolation of the quantitatively validated binary data and the simple model of *C*14, which is validated from the Mg-rich side.

The calculated isothermal section at 500 °C is presented in Fig. 7. Superimposed are the chemical compositions of the two DTA samples as well as the EPMA results of the chemical microanalysis of the phases in these samples. A substantial deviation between the measured and the

Table 7 Calculated phase compositions at the ternary eutectic reaction E1 (at 510 °C) of the Mg-Ca-Sr system

	Composition, wt.%		
Phase	**Mg**	**Ca**	**Sr**
L	79.54	13.14	7.32
(Mg)	99.28	0.59	0.13
$Mg_{17}Sr_2$	72.40	2.61	24.99
*C*14	51.30	36.89	11.82

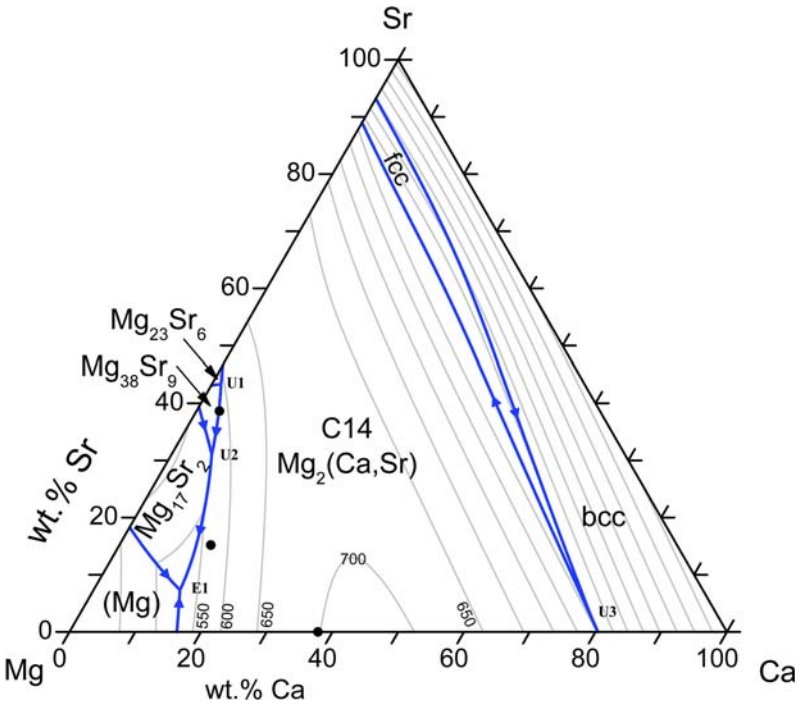

Fig. 6 Calculated liquidus projection of the Mg-Ca-Sr system. The solid dots (•) represent the sample compositions and the thin lines isotherms with an interval of 50 °C

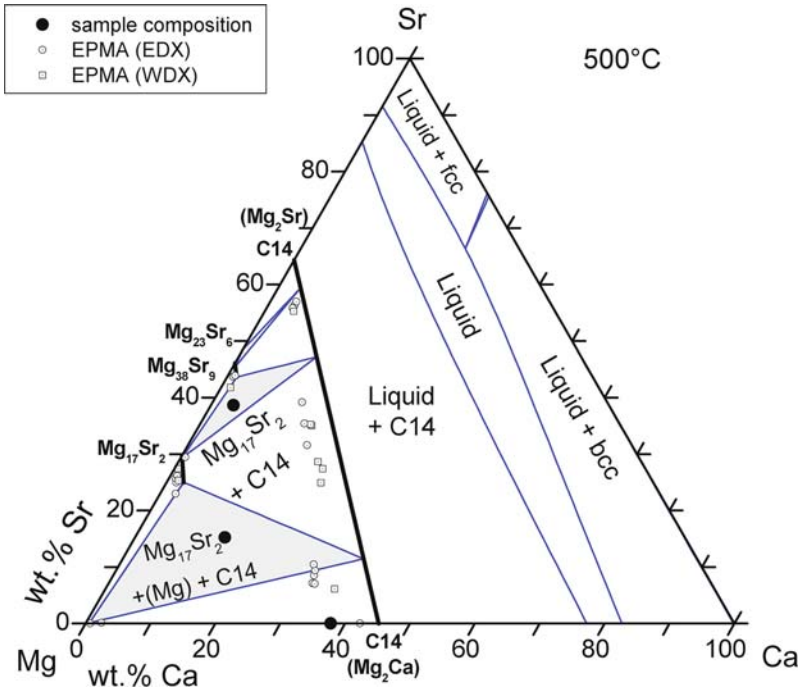

Fig. 7 Calculated isothermal Mg-Ca-Sr phase diagram section at 500 °C compared with experimental data from EPMA. The solid dots (•) represent the sample compositions; the grey areas indicate three-phase regions. Ternary solubilities of binary phases are highlighted with bold lines

calculated microchemical phase composition is visible for the *C*14 phase, suggesting an apparent solubility of Mg in this phase in addition to the interchangeable Ca and Sr. This shift in composition from the $(Mg)_2(Ca,Sr)$ section may be caused by detecting some of the Mg matrix together with the *C*14 visible on the surface in the micrograph. It is very unlikely that such a significant ternary Mg solubility occurs while still considering the binary end members of *C*14 as stoichiometric phases. However, an additional binary Mg-Ca sample at 38 wt.% Ca, also shown in Fig. 6 and solidified under the same conditions in DTA, suggested a small Mg solubility in *C*14-Mg_2Ca with a phase composition of 60Mg-40Ca (wt.%), measured by EDX. We do not have enough data for a corresponding quantitative revision of the Ca-Mg system, going beyond the binary stoichiometric Mg_2Ca phase assumed in Ref 11 and 17. Therefore we continue to use the simplified line compound description at constant Ca content for the ternary *C*14-$(Mg)_2(Ca,Sr)$ phase.

The cluster of EPMA data points for *C*14 near the Mg-Ca side is from sample MCS1, whereas the data in the center of the phase diagram *and* on the Mg-Sr side are from sample MCS2. This occurrence of *C*14 over a composition range has already been noticed in the *C*14 contrast in the microstructure of sample MCS2 in Fig. 2. This may be understood by considering the solidification of this sample under nonequilibrium conditions. Figure 8 shows the phase fraction and composition of *C*14 calculated under Scheil conditions. The variation of Mg composition is caused by the wt.% scale. It is obvious that the solidification starts with Sr-rich *C*14, and a significant monotonous decrease of Sr composition is expected. That is, in the *C*14-particles precipitating during ongoing solidification Sr is more and more substituted by Ca. This may very well explain the actually measured compositions in sample MCS2, ranging from 21 to 57 wt.% Sr for the particles shown in Fig. 2, from the earlier precipitated bright *C*14 particles to the later crystallizing darker ones. One may argue that the Scheil conditions might be too drastic for the quite slow solidification in DTA. However, a similar, at least qualitative, agreement has been clearly observed in Mg-Al-Mn-Zn alloys solidified at rates as low as 1 K/min.[18] In summary, the types of all phases observed in the microstructures of the two Mg-Ca-Sr samples are in full agreement with the calculated equilibrium results at subsolidus temperature.

Figure 9 shows a calculated vertical phase diagram section through the Mg-Ca-Sr system, crossing the composition of the two samples; the corresponding DTA thermal signals are superimposed. The calculated liquidus line in this diagram is quite flat, the thermal signal from sample MCS1 at 13.9 wt.% Ca suggests slightly higher temperatures. All other DTA signals of this sample are in very good agreement with the calculation, especially the important ternary eutectic at 510 °C in the Mg corner. The first signal of sample MCS2 at 3.5 wt.% Ca cannot be assigned to a reaction—it is close to the temperature of the metastable congruent melting point of $Mg_{38}Sr_9$ which is 600.2 °C. This strong peak in the heating curve might indicate a kinetic barrier for the transformations of $Mg_{38}Sr_9$ during heating.

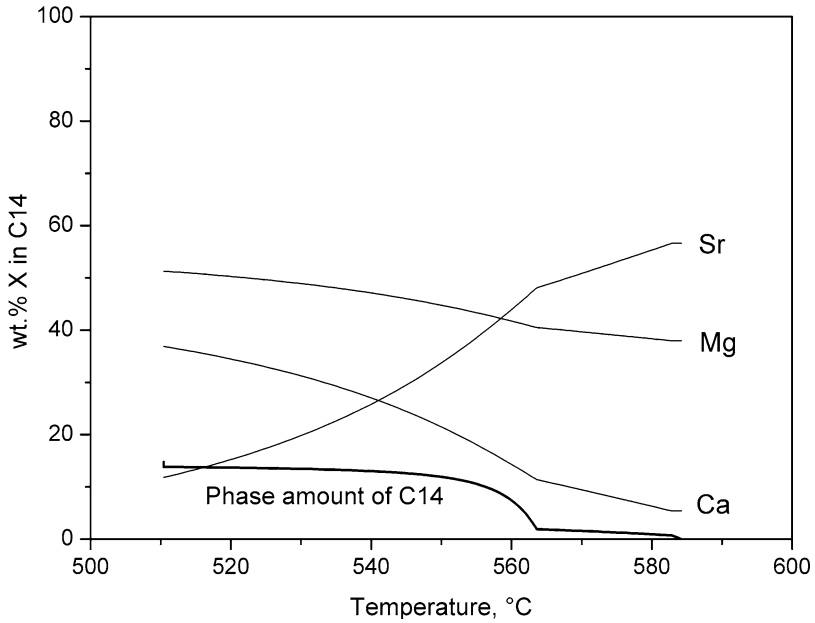

Fig. 8 Calculated change in composition of the C14 phase during solidification of sample MCS2 under Scheil conditions

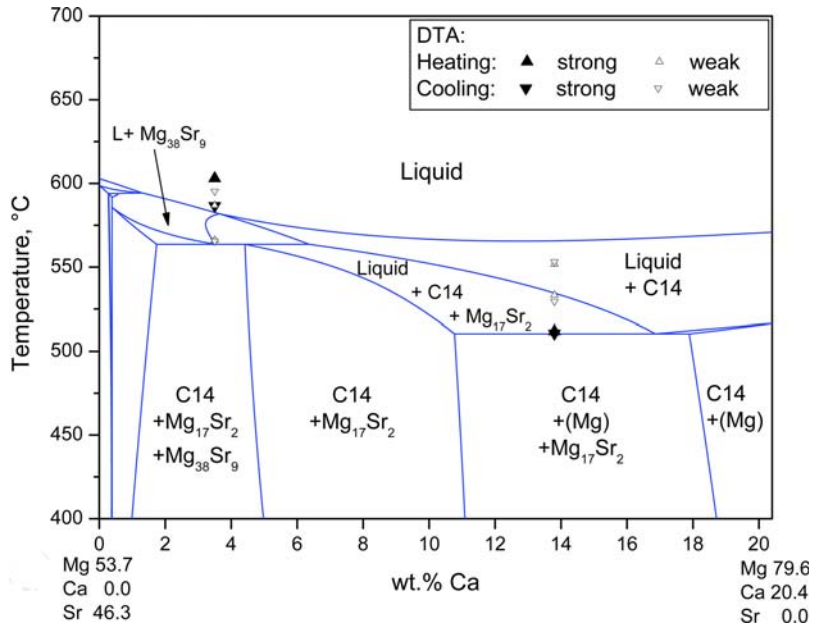

Fig. 9 Calculated vertical phase diagram section in the Mg-Ca-Sr system with experimental data from DTA

The other thermal signals are reasonably well reproduced by the calculation.

5.2 The Al-Ca-Sr Phase Equilibria

The projection of the calculated liquidus surface presented in Fig. 10 shows the *C*15-Al_2Ca phase as the predominant primary precipitate in the Al-Ca-Sr system. A number of invariant reactions of the transition type U, one ternary peritectic P, and one ternary eutectic E occur. The latter is calculated to appear at the very low temperature of 235 °C, which is 317 K below the lowest liquidus temperature in any of the binaries. Its location, with a Ca- and Sr-rich liquid phase at E, compounds the impression of very steep liquidus fields in that region indicated by the isotherms in Fig. 10.

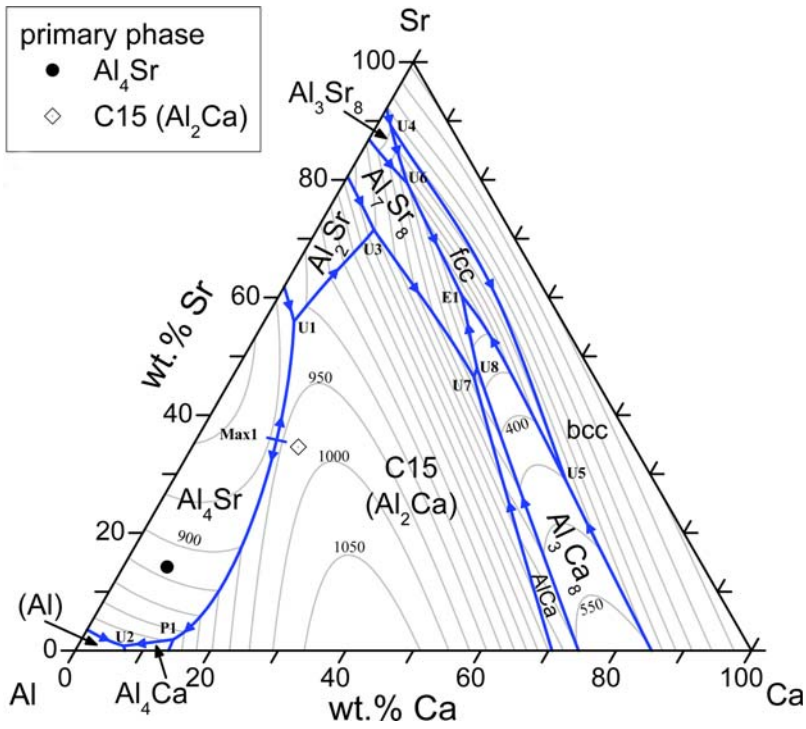

Fig. 10 Calculated liquidus projection of the Al-Ca-Sr system. The thin lines represent isotherms with an interval of 50 °C. Superimposed are experimentally determined primary phases

This behavior is caused by the limitation of the extrapolative calculation and the missing data for the ternary solubilities of the Al-poor phases AlCa, Al_3Ca_8, and Al_3Sr_8. Introducing ternary solubilities to these phases in the same order of magnitude as for the other binary phases would change these Al-poor phase equilibria drastically, shifting the resulting ternary eutectic reaction to a higher temperature. Since no experimental data are available in this Al-poor composition range, it was decided to not introduce speculative ternary solubilities for these three phases. This limitation is probably acceptable since only samples with less than 55 wt.% Al would be involved in these uncertain phase equilibria, posing substantial difficulties for experimental studies. The solidification path of Al-rich alloys, essentially above the composition of the maximum Max_1, will run down to the (Al) corner. This is the only maximum in the monovariant lines on the projection of the liquidus surface and is calculated to occur at 939 °C for the reaction $L \leftrightarrow Al_4Sr + C15$.

The calculated isothermal phase diagram section at 500 °C is presented in Fig. 11. Superimposed are the compositions of the three present samples (solid dots) and the results of the phase analysis with EPMA from this work and by XRD from Ref 5.

The huge ternary solubility of the $C15$-Al_2Ca phase is remarkable, extending almost to the binary Al-Sr edge and leaving only 10 wt.% Ca in $C15$. This incident and the narrow gap to the Al_2Sr phase was found by Zhang et al.[5] with XRD and is well supported by the present findings with EPMA. Only the combination of the results from XRD and EPMA enable a clear identification of this most Sr-rich phase composition and a distinction between the Al_2Sr and the $C15$ phase.

A substantial extension of an Al-poor liquid phase region is noted at 500 °C. This Ca-Sr-rich liquid field also exists at this temperature for the other ternary subsystem Mg-Ca-Sr. Introducing ternary solubilities for the Al-poor phases as discussed previously would significantly reduce this wide range of liquid phase stability.

The sample tempered at 500 °C, ACS2, has not attained equilibrium with the expected phases $Al_4Sr + Al_2Ca$ and possibly some Al_4Ca. The microstructure in Fig. 5 shows (Al), Al_4Sr, $C15$, and Al_7Sr_8; this suggests that the dense Al_4Sr layer acted like an inert barrier separating the (Al) in the upper part of the figure from the Sr-rich phases in the lower part. Most definitely, (Al) and Al_7Sr_8 cannot be in equilibrium. However, the ternary solubility of Ca in Al_7Sr_8 detected by EPMA has been used as an approximate value to introduce the Ca solubility in modeling that phase. Other than that, it is emphasized that the calculated phase equilibria in the area Ca-Sr-Al_2Sr-Al_2Ca are not supported by ternary experimental data. Since the overall composition of sample ACS2 had more Ca compared to any of the detected phases, an oxygen contamination may be assumed, suggesting that the somewhat grainy structure in the lower middle part of the image probably contains CaO.

In Fig. 12 the thermal signals from the two DTA samples are superimposed onto the calculated vertical phase diagram section. A quite reasonable agreement is

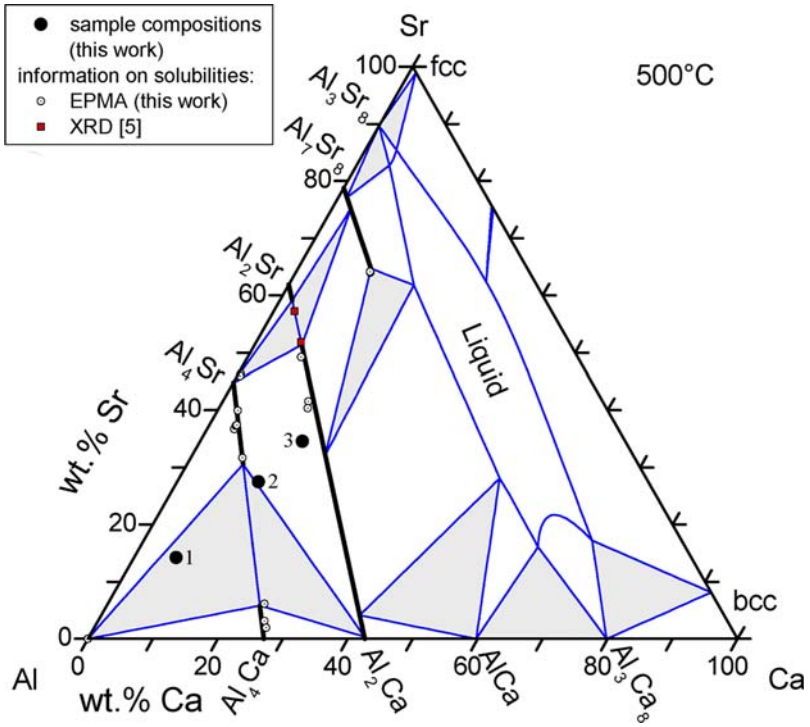

Fig. 11 Calculated isothermal Al-Ca-Sr phase diagram section at 500 °C. Superimposed are chemical compositions of the samples and phase analysis results with EPMA of this work and with XRD from Zhang et al.[5]

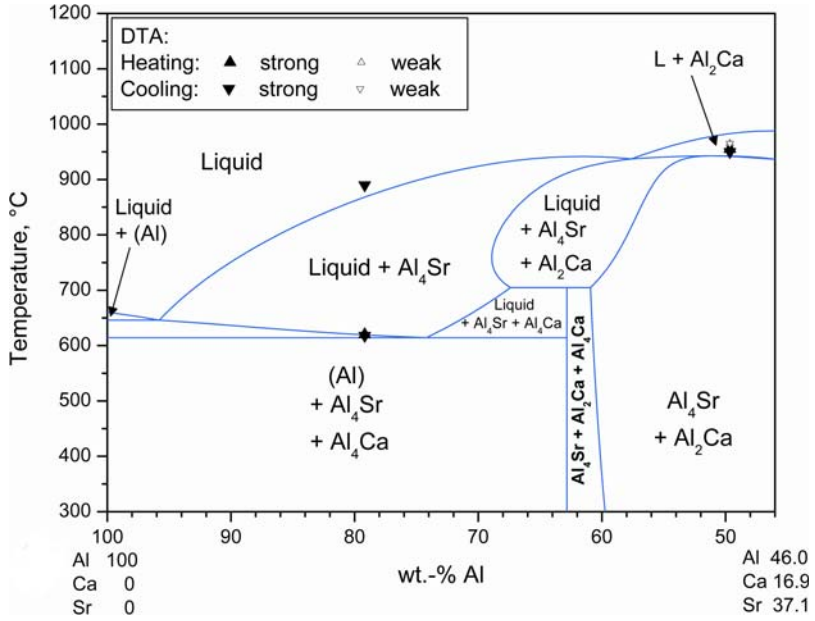

Fig. 12 Calculated vertical phase diagram section in the Al-Ca-Sr system. Superimposed are the thermal signals from samples ACS1 and ACS3

found for both samples, only the liquidus signal of sample ACS3 is lacking. The final phase assembly detected in these two samples in the microstructure is in good agreement with the calculated phase equilibria at subsolidus temperature.

6. Conclusion

Thermodynamic descriptions were developed for the Mg-Ca-Sr and the Al-Ca-Sr systems. For the first time, the

significant mutual ternary solid solubilities of pertinent intermetallic phases are quantitatively introduced and validated by experimental data.

- Key experiments with Mg-Ca-Sr alloys revealed the phase equilibria in the Mg-rich corner up to the *C*14 phase. The ternary solubilities of the binary Mg-Ca and Mg-Sr phases were evaluated. It was shown that the solidification of alloys with higher Ca and Sr content is nontrivial because of the complete mutual solubility in the *C*14 phase.
- In the Al-based system the very large ternary Sr solubility for the *C*15-Al_2Ca phase, proposed in Ref 5, was corroborated by the findings with EPMA. Significant mutual, though not complete, solid solubility was detected between the two phases Al_4Ca and Al_4Sr.
- Experimental work was limited to five selected key samples, and two of these are not in equilibrium. Therefore reported results, while representing progress with respect to the previous knowledge, are affected by a relatively high level of uncertainty.

Acknowledgment

This study is supported by the German Research Foundation (DFG) in the Priority Programme "DFG-SPP 1168: InnoMagTec."

References

1. R. Schmid-Fetzer, J. Groebner, D. Mirkovic, A. Janz, and A. Kozlov, Constitution of Magnesium Alloys, *Magnesium Technology 2007*, R. Beals, M. Pekguleryuz, and N. Neelameggham, Eds., TMS (The Minerals, Metals & Materials Society), 2007, p 339-344
2. J. Ågren, F.H. Hayes, L. Höglund, U.R. Kattner, B. Legendre, and R. Schmid Fetzer, Applications of Computational Thermodynamics, *Z. Metallkd.*, 2002, **93**, p 128-142
3. A. Janz, J. Gröbner, H. Cao, J. Zhu, Y.A. Chang, and R. Schmid-Fetzer, Thermodynamic Modeling of the Mg-Al-Ca System, *Acta Mater.*, 2008, **57**(3), p 682-694
4. A. Janz, J. Gröbner, D. Mirkovic, M. Medraj, J. Zhu, Y.-A. Chang, and R. Schmid-Fetzer, Experimental Study and Thermodynamic Calculation of Al-Mg-Sr Phase Equilibria, *Intermetallics*, 2007, **15**(4), p 506-519
5. Q.A. Zhang, H. Enoki, and E. Akiba, Phase Relations and Hydrogenation Behavior of $Sr_{1-x}Ca_xAl_2$ ($0 \le x \le 1$), *J. Alloy. Compd.*, 2001, **322**, p 257-264
6. Y. Zhong, J.O. Sofo, A.A. Luo, and Z.-K. Liu, Thermodynamics Modeling of the Mg-Sr and Ca-Mg-Sr Systems, *J. Alloy. Compd.*, 2006, **421**, p 172-178
7. M. Aljarrah and M. Medraj, Thermodynamic Modelling of the Mg-Ca, Mg-Sr, Ca-Sr and Mg-Ca-Sr Systems Using the Modified Quasichemical Model, *Calphad*, 2008, **32**, p 240-251
8. M. Aljarrah and M. Medraj, Thermodynamic Assessment of the Phase Equilibria in the Al-Ca-Sr System Using the Modified Quasichemical Model, *J. Chem. Thermodyn.*, 2008, **40**(4), p 724-734
9. A. Janz, J. Gröbner, and R. Schmid-Fetzer, Thermodynamics and Constitution of Mg-Al-Ca-Sr-Mn Alloys: Part II: Procedure for Multicomponent Key Sample Selection and Application to the Mg-Al-Ca-Sr and Mg-Al-Ca-Sr-Mn Systems, *J. Phase Equilib. Diffus.*, 2009. doi:10.1007/s11669-009-9468-3
10. D. Mirković and R. Schmid-Fetzer, Solidification Curves for Commercial Mg Alloys Obtained from Heat Transfer Modeled DTA Experiments, *Z. Metallkd.*, 2006, **97**, p 119-129
11. A. Kozlov, M. Ohno, R. Arroyave, Z.K. Liu, and R. Schmid-Fetzer, Phase Equilibria, Thermodynamics and Solidification Microstructures of Mg-Sn-Ca Alloys—Part 1. Experimental Investigation and Thermodynamic Modeling of the Ternary Mg-Sn-Ca System, *Intermetallics*, 2008, **16**(2), p 299-315
12. S.-L. Chen, S. Daniel, F. Zhang, Y.A. Chang, W.-A. Oates, and R. Schmid-Fetzer, On the Calculation of Multicomponent Stable Phase Diagrams, *J. Phase Equilib.*, 2001, **22**, p 373-378
13. S.-L. Chen, S. Daniel, F. Zhang, Y.-A. Chang, X.-Y. Yan, F.-Y. Xie, R. Schmid-Fetzer, and W.-A. Oates, The Pandat Software Package and its Applications, *Calphad*, 2002, **26**, p 175-188
14. A.T. Dinsdale, SGTE Data for Pure Elements, *Calphad*, 1991, **15**, p 317-425
15. M. Hillert, The Compound Energy Formalism, *J. Alloy. Compd.*, 2001, **320**, p 161-176
16. A. Janz, "Thermodynamics and Constitution of Quaternary Mg-Al-Ca-Sr Alloys and the Extension to the Quinary Mg-Al-Ca-Sr-Mn System," Ph.D. thesis (Dr.-Ing., 28 March 2008), Clausthal University of Technology, Germany, 2008
17. R. Agarwal, J. Lee, H. Lukas, and F. Sommer, Calorimetric Measurements and Thermodynamic Optimization of the Ca-Mg System, *Z. Metallkd.*, 1995, **86**(2), p 103-108
18. M. Ohno, D. Mirkovic, and R. Schmid-Fetzer, Liquidus and Solidus Temperatures of Mg-rich Mg-Al-Mn-Zn Alloys, *Acta Mater.*, 2006, **54**, p 3883-3891
19. D. Kevorkov, R. Schmid-Fetzer, A. Pisch, F. Hodaj, and C. Colinet, The Al-Ca System: Part 2: Calorimetric Measurements and Thermodynamic Assessment, *Z. Metallkd.*, 2001, **92**, p 953-958
20. Y. Zhong, C. Wolverton, Y. Austin Chang, and Z.-K. Liu, A Combined CALPHAD/First-Principles Remodeling of the Thermodynamics of Al-Sr: Unsuspected Ground State Energies by "Rounding Up the (Un)usual Suspects", *Acta Mater.*, 2004, **52**, p 2739-2754
21. Y. Zhong, K. Ozturk, and Z.-K. Liu, Thermodynamic Modeling of the Ca-Sr-Zn Ternary System, *J. Phase Equilib.*, 2003, **24**, p 340-346